Comparison of Field-To-Line Coupling Models: Coupled Transmission Lines Model versus Single-cell Corrected Taylor Model

Sjoerd Op 'T Land, Tvrtko Mandić, Mohamed Ramdani, Adrijan Barić, Richard Perdriau, Bart Nauwelaers

Comparison of Field-To-Line Coupling Models: Coupled Transmission Lines Model versus Single-cell Corrected Taylor Model

Sjoerd Op 't Land*, Tvrtko Mandić†, Mohamed Ramdani*, Adrijan Barić†, Richard Perdriau* and Bart Nauwelaers‡
*Department of Electronics, Ecole Superieure d'Electronique de Ouest, Angers, France
Email: {sjoerd.optland, mohamed.ramdani}@eseo.fr
†Faculty of Electrical Engineering and Computing (FER), University of Zagreb, Croatia
Email: {tvrtko.mandic, adrijan.baric}@fer.hr
‡Department of Electrical Engineering (ESAT), KU Leuven, Belgium
Email: bart.nauwelaers@esat.kuleuven.be

***Abstract*—Models for field-to-line coupling are interesting because they help to predict the immunity of PCBs and explain the relation between routing and immunity. In this article a meandered PCB trace illuminated by EM field in a TEM cell is analysed. The near-end and far-end coupling is predicted using two models: a detailed and an approximative one. The detailed model is a circuit of coupled multi-conductor transmission lines evaluated with a circuit simulator. The approximative model consists of a single Taylor cell with an analytical modification evaluated using a numerical computing tool. Both predictions are compared with measurements and turn out to be equally precise. The advantage of the coupled lines model is its flexibility, the advantage of the modified Taylor model is its ease of use.**

***Index Terms*—EMC, immunity, field-to-line coupling, microstrip, PCB, TEM cell, GTEM cell**

I. Introduction

The radiated immunity of electronic devices is commonly measured in a (gigahertz) transversal electromagnetic mode (GTEM) cell, which illuminates the Device Under Test (DUT) with a linearly polarized plane wave. The DUT is illuminated with a prescribed field strength at different frequencies, and the proper functioning of the DUT is monitored. If the DUT fails at any moment during the test, the designer should try to understand why, improve the design accordingly, produce a new prototype and test again. To reduce the number of expensive prototyping cycles, the designer strives to get the design First Time Right (FTR). To that end, the designer needs models that *predict* the immunity of the device. If the predicted or measured immunity is unsatisfactory, the model should *explain* which design parameters could be tuned to improve the immunity of the device.

Collaterally, these models should not be too expensive to employ. The financial investment in tools, and time necessary to explain, create and use the models should be reasonable. Quantitatively put, they should have a positive Return On Modelling Effort (*ROME*).

Electronic devices commonly consist of one or more Printed Circuit Boards (PCBs). PCBs contain components and traces to interconnect them. A typical failure can be understood as follows: a trace converts the incident field in a terminal voltage that causes the connected component to fail. To predict and explain this failure, the models of the trace and components are needed. The trace model describes how well it picks up the incident field, as a function of its geometry. The component model describes at which terminal voltage it starts to fail. The immunity can thus be improved by picking a component with better immunity or by drawing a trace that performs as less efficient antenna. The latter might be an easier solution, because the PCB designer can play with trace layout autonomously. Therefore, we will concentrate on trace models.

To illustrate the problem and to direct the rest of the study, we will first define a test case in section II. Then, we will give an overview of existing models in section III. From the available models, we select a detailed model and an approximate model, and explain them in section IV and V, respectively. Their predictions will be compared to the measurement in section VI and we conclude on them in section VII, estimating their respective *ROMEs*.

II. Test Case

Let us now design a realistically complex PCB trace that allows for coupling measurement. The trace should be complex to challenge field-to-trace models. Yet, it should not have too many non-idealities in order to explain discrepancies between the model and measurements. We will first describe the complexity of typical PCB traces and then simplify.

Typical PCB traces meander with 90^o and 45^o bends. Width changes and none-chamfered bends introduce impedance discontinuities. On typical 2-layer PCBs, traces can be considered as MS (microstrip) lines above a ground plane. On multi-layer PCBs, copper floods to the left and right of a trace make for

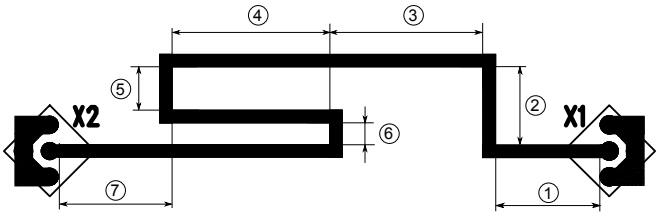

(a) Meander MS line having uniform width $w = 1.75\,\text{mm}$ manufactured on 1 mm FR-4 substrate.

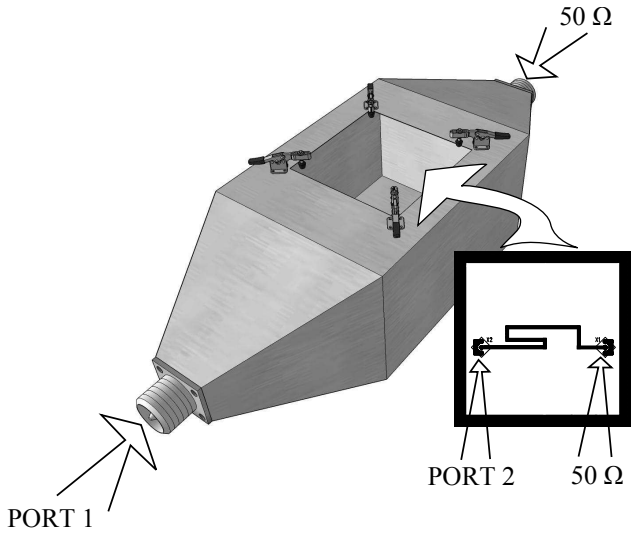

(b) Measurement set-up.

Figure 1. Test case used for modelling field-to-line coupling.

a CPW (coplanar waveguide) or GCPW (grounded coplanar waveguide).

We design a MS line trace with non-chamfered 90° bends. To simplify measurement of the induced terminal voltages, we matched the line to the measurement set-up characteristic impedance of 50 Ω.

The resulting MS line presented in Figure 1 is manufactured on an FR-4 substrate having the dimensions $10 \times 10\,\text{cm}$. The dimensions are set to fit the TEM cell square opening. The MS line is connected by 3-pin through-hole SMA connectors. The presented transmission line has the uniform width of 1.75 mm and the thickness of the substrate is 1 mm.

The coupling between the TEM cell and the transmission lines are characterized by VNA measurements according to the set-up shown in Figure 1b. The coupling measurements are performed by a two-port VNA connected to the TEM cell signal input port and to the one end of the transmission line. The second TEM cell port, as well as the second transmission line port are terminated in 50 Ω. The measurements of the near-end coupling are performed as shown in Figure 1b. The far-end coupling measurements are performed by terminating the other port of the transmission line.

The length of the transmission line sections are presented in Table I. These lengths do not take into account the line bends.

Table I
GEOMETRICAL PARAMETERS OF THE MS LINE PRESENTED IN FIGURE 1A.

Section no.	1	2	3	4	5	6	7
l (mm)	14.5	10.75	19.5	21.75	6	3	14

III. STATE OF THE ART

With the test case in mind, we will give an overview of the available models. We start with truthful but costly models working our way down to approximative but cheap models.

In general, Maxwell's equations do not have closed-form solutions. Full-wave solvers allow the definition of the substrate, an arbitrarily shaped trace and the illumination of the TEM cell. The advantage is that the traces can be imported from PCB design tools directly. Moreover, the real (non-uniform) field generated by the TEM cell is taken into account. However, it takes some time to set-up and run the simulation. If a designer wants to play with the routing and the illumination direction, time-expensive sweeps are needed. Furthermore, numerical solvers do not greatly help to *understand* which design parameters influence the coupling because slow simulation process.

A great class of models based on the simplification is using transmission line theory: the hypothesis of one differential TEM mode.

Commonly used ground planes create a virtual return trace, thereby suppressing the common mode. Furthermore, the contribution of the common mode to terminal voltages is low [1], [2]. Therefore, it is reasonable to neglect the common mode. As for the TEM mode, the quasi-TEM propagation mode of the microstrip transmission line is maintained up to [3]

$$f_{\text{MS,TEM}} \approx \frac{21.3\,\text{GHz}\cdot\text{mm}}{(w+2h)\sqrt{\varepsilon_r+1}} \approx 2.42\,\text{GHz}, \qquad (1)$$

which is in our case of a 1.75 mm wide microstrip line on a 1 mm thick substrate ($\varepsilon_r = 4.5$). The TEM cell itself can also be modelled as a transmission line. Its TEM propagation mode is maintained up to 1.65 GHz (cf. subsection VI-A).

Considering all trace segments and TEM cell itself as transmission lines, one can calculate the total coupling using MTL (multi-conductor transmission line) theory [4]. This strongly coupled approach is taken in section IV.

The weakly coupled approach considers the incident field unchanged by the presence of the microstrip line. The equivalent models of Taylor et al. [5], Agrawal et al. [6] and that of Rachidi [7] are based on this assumption. They incorporate the incident field by adding controlled voltage and/or current sources to the *rglc* lumped-element transmission line model. If the line becomes electrically long, it needs to be meshed in an increasing number of cells in order to remain accurate.

Alternatively, every line segment can be modelled as a single lumped-element cell with a correction factor for long-line effects [8]. This model potentially improves understanding and allows for short design-simulation cycles.

This approach is taken in section V.

Finally, the incident field can be considered uniform, thereby avoiding meshing and improving understanding. This approach should be valid as long as the maximum dimension of the illuminated structure remains a fraction of the wavelength ($\lambda/10$, for example). In our case ($d = 72 \times 14\,\text{mm}$), this quasi-static model should hold up to

$$f_{\text{QS}} = \frac{\text{c}_0}{10\ d_{\max}} \approx 0.4\,\text{GHz}. \tag{2}$$

IV. Coupled Transmission Lines Model

The Method of Lines (MoL) is a 2D semi-numerical method that is very efficient in solving EM differential equations related to microwave structures [9], [10]. The method allows for fast calculation of the coupling capacitance between the transmission line and the TEM cell by using quasi-static approach [11]. The quasi-static approach is found to be suitable for modelling the TEM cell and transmission line EM coupling by considering the per-unit-length (p.u.l) parameters [4]. The capacitance matrix for the n-conductor transmission line calculated by MoL can be written as

$$C = \begin{bmatrix} C_{11} & C_{12} & \cdots & C_{1n} \\ C_{21} & C_{22} & \cdots & C_{2n} \\ \vdots & \vdots & \ddots & \vdots \\ C_{n1} & C_{n2} & \cdots & C_{nn} \end{bmatrix}. \tag{3}$$

For the case of the multi-conductor transmission line (MTL) inserted in the TEM cell, the n^{th}-conductor is the TEM cell itself. Therefore, the capacitance C_{nn} represents the self capacitance of the TEM cell, while the capacitances C_{in} or C_{ni}, $i = 1 \ldots n-1$ are the coupling capacitances between the septum of the TEM cell and the each transmission line. After obtaining the capacitance matrix C for the given MTL, it is possible to calculate the inductance matrix L as [12]

$$L = \mu_0 \varepsilon_0 C_0^{-1} \tag{4}$$

where C_0 is the free-space capacitance matrix, i.e. the matrix obtained by simulation of the structure having all dielectric constants set to 1. Therefore, for the planar structure having at least one dielectric constant which is not 1, two MoL simulations are needed in order to obtain the capacitance and inductance matrix.

The calculated C and L matrices can be used as input for the MTL component available in many SPICE-like circuit simulators, i.e. *W*-elements. Nevertheless, the coupling parameters must be modified with respect to the transmission line position in the TEM cell. The coupling capacitances are always present due to the nature of *E*-field lines in the TEM cell and therefore require no modification, while the coupling inductances require modification. The coupling inductances L_{ij} should be multiplied by the cosine of the angle α between the TEM cell longitudinal axis and the transmission line [4]. Furthermore, the self capacitance and self inductance of the TEM cell are also multiplied by cosine of the angle α to accurately model the phase variation through the TEM cell.

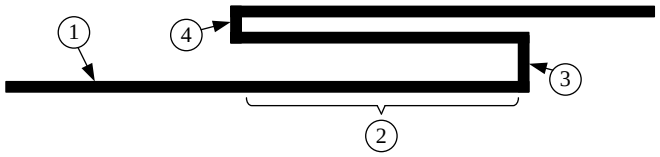

(a) Example of MS transmission line.

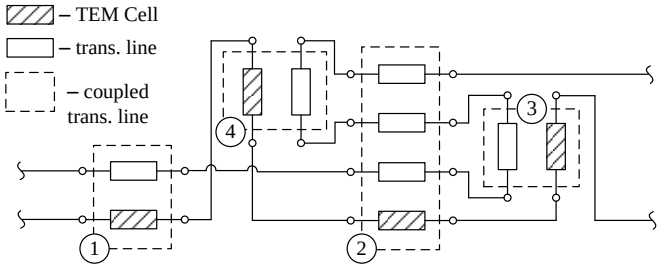

(b) Circuit model obtained by segmentation of transmission line.

Figure 2. Modelling of EM coupling by coupled transmission lines.

This means that the transversally positioned transmission line ($\alpha = 90°$) will have only the coupling capacitance defined.

Figure 2 shows the application of the presented procedure on an arbitrarily shaped transmission line. The transmission line presented in Figure 2a is segmented into several sections. For each section the matrices C and L are calculated. The calculated matrices are used as inputs to the MTL components presented in Figure 2b.

V. Modified Taylor Model

The second field-to-line coupling model is based on that of Taylor [5]. Taylor's model can be understood as a Telegrapher's *rglc* lumped element model, with distributed sources that represent the electrically and magnetically induced currents and voltages (cf. Figure 3b).

For low frequencies, a straight microstrip segment can be modelled as a single Taylor's cell, because the field is uniform along the line. Neglecting the *rglc* elements and for the case of characteristic termination ($R_{\text{ne}} = R_{\text{fe}} = Z_c$), the both terminal voltages can be found by inspection:

$$V_{\text{LF}} = \pm\frac{1}{2}\text{j}\omega\mu_0 H_n^i h\ell - \frac{1}{2} Z_c \text{j}\omega c E_t^i h\ell, \tag{5}$$

where c is the per-unit-length capacity of the line, h the substrate thickness, ℓ the segment length and H_n^i and E_t^i the normal magnetic and transverse electric components of the incident electromagnetic field. Unless otherwise noted, expressions are given for the far-end and near-end where the positive sign is valid for the far-end and the negative sign for the near-end.

As the frequency rises, the field is no longer uniform along the line. Taylor's model is then applied by meshing the line in shorter cells, such that the field can be considered uniform again along each cell. The terminal voltages can then be found using a circuit simulator.

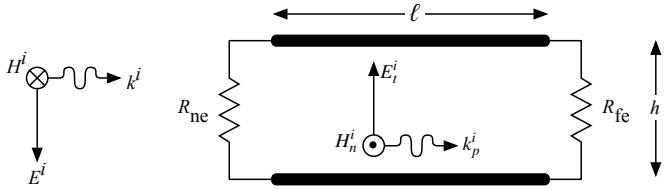

(a) End-fire illumination of a bifilar transmission line. The i superscript denotes the incident wave. The subscripts n, t and p denote field components normal, transversal and parallel to the line segment, respectively.

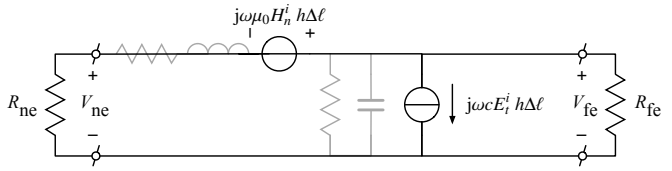

(b) Equivalent circuit model of the line, using only one Taylor's cell ($\Delta\ell = \ell$).

Figure 3. Taylor's model for field-to-line coupling.

Here, we choose another method to account for long line effects as proposed by Op 't Land [8]. Even for high frequencies, it consists of single Taylor's cell, but with an analytical correction factor to compensate for the introduced error. This correction factor K describes the correlation between the incident wave and the line's eigenwave, averaged along the segment length ℓ:

$$K = \frac{1}{\ell}\int_0^{\ell} \text{line} \cdot \text{incident}^*\ \mathrm{d}z, \tag{6}$$

where 'line' and 'incident' are the complex amplitudes of the line eigenwave and the incident plane wave and where z denotes path length along the segment. When illuminating one straight segment as shown in Figure 3a, this integral evaluates as:

$$K = \frac{1}{\ell}\int_0^{\ell} \mathrm{e}^{\mp \mathrm{j}k^{\mathrm{line}}z}\mathrm{e}^{+\mathrm{j}k^i z}\ \mathrm{d}z = \frac{1}{\mathrm{j}\left(k^i \mp k^{\mathrm{line}}\right)\ell}\left(\mathrm{e}^{\mathrm{j}\left(k^i \mp k^{\mathrm{line}}\right)\ell} - 1\right), \tag{7}$$

where k^{line} is the line wave number and k^i is the incident wave number. Indeed, the frequency where this factor first becomes zero depends on the velocity difference between the incident wave and the line eigenwave.

In the case of a multi-segment line, the correction factor for each segment s can be generalised as [8]:

$$K_s = \frac{1}{\mathrm{j}\left(\pm k^{\mathrm{line}} - k_{p,s}^i\right)\ell_s}\left(\mathrm{e}^{\mathrm{j}(\varphi_{\mathrm{end}} - \theta_{\mathrm{end}})} - \mathrm{e}^{\mathrm{j}(\varphi_{\mathrm{begin}} - \theta_{\mathrm{begin}})}\right), \tag{8}$$

where ℓ_s is the segment length and $k_{p,s}^i$ is the incident wave vector parallel to the segment, φ the incident field phase and θ the line eigenwave phase. Both φ and θ are referenced zero at the beginning of the first segment.

To find the near-end and far-end induced voltages, the contributions of the different segments need to be summed:

$$V = \sum_{s=1}^{N} K_s \cdot V_{s,\mathrm{LF}}. \tag{9}$$

In the far-end case, the line propagation delay needs to be added to move the phase reference from the near-end to the far-end.

To evaluate this formulation in this case of a TEM cell and a microstrip, the field strengths are approximated by

$$E_t^i = \frac{1}{\varepsilon_r}\frac{V_{\mathrm{septum}}}{h_{\mathrm{septum}}} \tag{10}$$

$$H^i = \frac{1}{\eta}\frac{V_{\mathrm{septum}}}{h_{\mathrm{septum}}}, \tag{11}$$

because the line mainly 'feels' the field in the substrate and we suppose the relative permeability $\mu_r = 1$.

To find k^{line}, we use any microstrip line calculator that yields the effective permittivity $\varepsilon_{r,\mathrm{eff}} = 3.5$. From there, we find the phase speed $v^{\mathrm{line}} = \mathrm{c}_0/\sqrt{\varepsilon_{r,\mathrm{eff}}}$, $k^{\mathrm{line}} = \omega/v^{\mathrm{line}}$ and the per-unit-length capacity $c = 1/(Z_c v^{\mathrm{line}})$. If we take $V_{\mathrm{septum}} \equiv 1\,\mathrm{V}$, the calculated terminal voltages will equal the voltage transfer between the septum and terminal. Moreover, because the TEM cell and the network analyser have $50\,\Omega$ inputs, the voltage transfer will equal the S_{21} parameter.

The closed-form prediction can be evaluated with a numerical tool like MATLAB, Scilab or a graphing calculator. For this paper, the predictions are performed with a Python script [13]. This same script performs the comparison with the measurements and thus reproduces the main results of this paper.

If the user has these tools at hand and knows how to use them, it takes only several minutes to enter the model and several seconds to run the simulation.

VI. Results

The test PCB described in section II is produced, and the transfer from the TEM cell input to the far-end was measured using a network analyser. The near-end of the test PCB was terminated using a broadband $50\,\Omega$ load. The resulting S_{21} is shown in Figure 4a. The near-end transfer was measured in the same way and is shown in Figure 4b.

We will first explain the transfer peaks above 1 GHz and then summarise the precision of both models.

A. TEM Cell Resonances

The higher-order modes of propagation can propagate within the TEM cell above their respective cut-off frequencies. These propagation modes impose limitation on the TEM cell useful frequency range because of the presence of resonances as well as multi-moding. The first several higher-order modes are transverse electric (TE) modes. For the small gap TEM cells or when the aspect ratio of the TEM cell width and height is smaller than 1.92 [14] the first higher-order propagating mode is TE_{01}. This mode is largely confined to the gap area and does not significantly affect the TEM mode field distribution in the usual test region [15]. The wavelength of

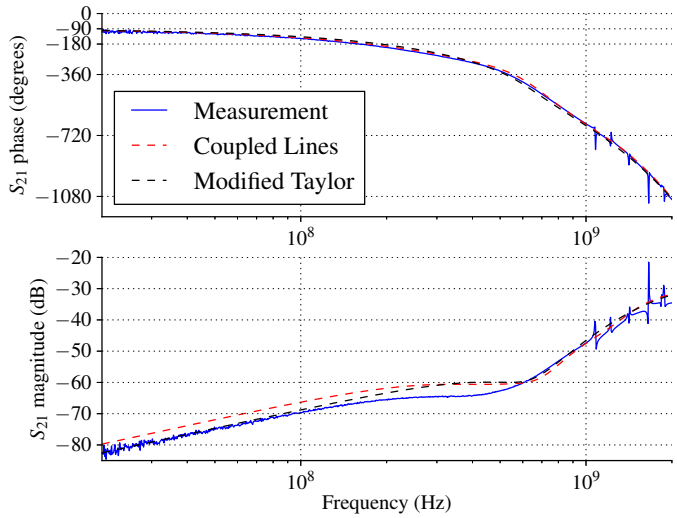

(a) Far-end coupling.

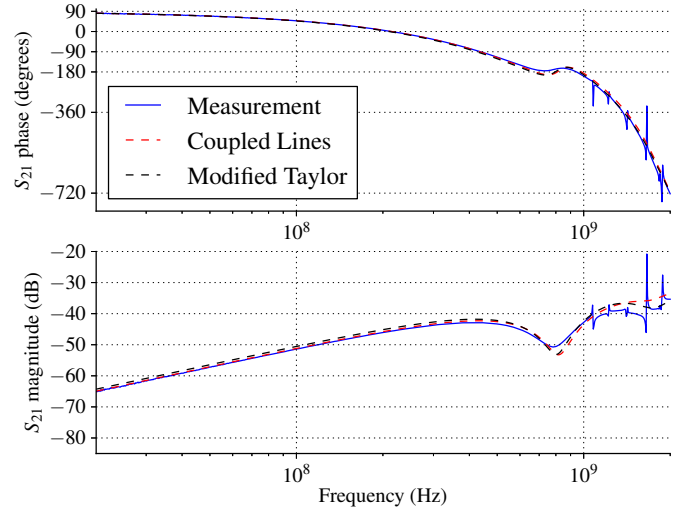

(b) Near-end coupling.

Figure 4. Comparison between measurement and both models.

the first cut-off frequency for the FCC-TEM-JM2 cell can be calculated by [14]

$$\lambda_{c(01)} = 2a/(0.488a/b + 0.0626) = 0.342\,\mathrm{m} \tag{12}$$

where a and b are the TEM cell width and height, respectively. The second propagating mode is TE_{10} and the respective cut-off wavelength can be calculated as

$$\lambda_{c(10)} = 2a = 0.296\,\mathrm{m} \tag{13}$$

The cut-off frequencies of the propagation modes TE_{01} and TE_{10} are

$$f_{c(01)} = \mathrm{c}_0/\lambda_{c(01)} = 877\,\mathrm{MHz}, f_{c(10)} = \mathrm{c}_0/\lambda_{c(10)} = 1.01\,\mathrm{GHz}, \tag{14}$$

where c_0 is the speed of light in vacuum.

The TEM cell is a high-Q cavity and therefore resonances are sharp and exist only in a very narrow frequency range. For specific applications, the TEM cell could still be used in the

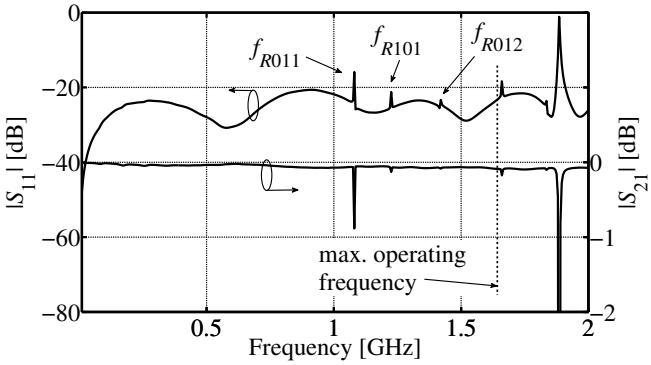

Figure 5. TEM cell measurements of the parameters S_{11} and S_{21}. First three resonant frequencies are identified.

frequency range between the resonances [16]. Nevertheless, at the resonant frequency the energy in the corresponding TE mode is high and the longitudinal magnetic field component is also relatively high. These conditions significantly distort the magnitudes of the transversal field components.

The higher-order modes undergo multiple reflections due to the tapered sections of the TEM cell. The position of the reflection within the taper is different for each higher-order propagating mode and it is determined by the point where the taper cross-section is too small to support the propagation. The resonant frequency can be calculated as [17]

$$f_{R(mnp)} = \sqrt{f_{c(mn)}^2 + \left(\frac{p\mathrm{c}_0}{2L_{mn}}\right)^2}, \tag{15}$$

where $f_{c(mn)}$ is the cut-off frequency of the higher-order (m,n) mode and p is the multiplier $p = 1,2,3,\ldots$ for the half-guide wavelengths at which the resonance occurs. The effective resonant length L_{mn} is different for each propagating mode and can be calculated as

$$L_{mn} = l_c + 2l_e \cdot X_{mn}, \tag{16}$$

where l_c is the length of the TEM cell central section while l_e is the length of a taper. The parameter X_{mn} is a mode-dependent fraction $(0 < X_{mn} < 1)$ and there is no analytical solution up to now. In [18] empirical results for X_{mn} are given. For the TEM cell defined by $a/b = 1.67$ and $w/a = 0.72$ (very similar to the aspect ratios of the FCC-TEM-JM2) the parameter X_{mn} for the modes TE_{01} and TE_{10} is equal to 0.81 and 0.49, respectively. Using the cut-off frequencies calculated in (14) several resonant frequencies can be calculated as

$$f_{R(011)} = 1.05\,\mathrm{GHz}, f_{R(101)} = 1.24\,\mathrm{GHz}, f_{R(012)} = 1.45\,\mathrm{GHz}, \tag{17}$$

In Figure 5 the measurements of the parameters S_{11} and S_{21} are presented. Three resonances can be observed below the specified operating frequency range of 1.65 GHz. It should be mentioned that the propagation mode resonance can exist even if there is no resonance present in the measured S-parameters [18]. In the operating frequency range the resonances are identified at the frequencies 1.08 GHz, 1.22 GHz and 1.42 GHz.

Table II
COMPARISON BETWEEN COUPLED LINES AND MODIFIED TAYLOR FIELD-TO-LINE COUPLING MODELS.

Model	Coupled Lines	Modified Taylor
Cell information	septum size and position, tapering	E_{avg}
Trace information	trace shape, h, w, ε_r	trace shape, h, ε_r, $\varepsilon_{r,\text{eff}}$
Supported trace types	multiple microstrip and coplanar traces	single microstrip
Discontinuity modelling	as lumped elements	impossible
Tools	ADS (or Qucs, Cadence)	Python (or MATLAB), microstrip calculator
Modelling time	10 minutes	minutes
Simulation time	seconds	seconds
Precision	+1.4 dB average	+1.1 dB average
in case study	1.0 dB avg. deviation	0.9 dB avg. deviation
Precision in general	inter-trace coupling modelled	inter-trace coupling neglected

The calculated resonant frequencies match the measured ones very well. Nevertheless, the reliable identification of the resonant frequencies can only be done by measuring simultaneously the S-parameters and the E-field strength inside the TEM cell [18].

B. Precision

As a measure of the systematic bias, we took the log-frequency average of the difference model-prediction in dB. Because of the low frequency measurement noise and because the high frequency interesting phenomena, we only used the data from 20 MHz upward. We calculated this average error for both the near-end and the far-end measurement and took the average again.

As a measure of the uncertainty, we took the error in dB, subtracted the average error (bias), took the absolute value and averaged over the log-frequency from 20 MHz upward. The results of both metrics are given in Table II.

VII. CONCLUSIONS AND RECOMMENDATIONS

This paper presents the comparison of the two methods for modelling the field-to-line coupling. The modified Taylor method presents the faster way for the estimation of the induced voltages at the transmission line ends. The coupled lines method employs 2D solver to calculate the capacitance and inductance matrix and therefore requires an additional time effort. However, this method is easily applicable to the multiconductor transmission lines. Both methods are compared to the measurements performed for the meander MS line having 90^{o} bends illuminated by EM field generated by the TEM cell. Both methods are very accurate up to the cut-off frequency of the TEM cell. The difference between the models and the measurements is largest at the resonant frequencies of the TEM cell. These frequencies are successfully identified and analysed.

The future work will focus on modelling of EM field coupling to the more realistic PCB transmission lines. The modelling will be performed on PCB lines having impedance discontinuities such as ground slots, MS-to-CPW transitions, arbitrarily bent lines, etc.

REFERENCES

[1] C. A. Nucci, F. Rachidi, and M. Rubinstein, "An overview of field-to-transmission line interaction," *Applied Computational Electromagnetics Society Newsletter*, vol. 22, no. 1, pp. 9–27, 2007.

[2] C. R. Paul, *Introduction to Electromagnetic Compatibility*. Wiley, 2006.

[3] K. H. Reinmut, *Handbook of microwave integrated circuits*, 1st ed. Norwood, MA: Artech House, Inc., 1987.

[4] T. Mandić, R. Gillon, B. Nauwelaers, and A. Barić, "Characterizing the TEM cell electric and magnetic field coupling to PCB transmission lines," *Electromagnetic Compatibility, IEEE Transactions on*, vol. 54, no. 5, pp. 976 –985, oct. 2012.

[5] C. D. Taylor, R. Satterwhite, and C. W. Harrison, Jr., "The response of a terminated two-wire transmission line excited by a nonuniform electromagnetic field," *Antennas and Propagation, IEEE Transactions on*, vol. 13, no. 6, pp. 987 – 989, nov 1965.

[6] A. K. Agrawal, H. J. Price, and S. H. Gurbaxani, "Transient response of multiconductor transmission lines excited by a nonuniform electromagnetic field," *Electromagnetic Compatibility, IEEE Transactions on*, vol. EMC-22, no. 2, pp. 119–129, 5 1980.

[7] F. Rachidi, "Formulation of the field-to-transmission line coupling equations in terms of magnetic excitation field," *Electromagnetic Compatibility, IEEE Transactions on*, vol. 35, no. 3, pp. 404 –407, aug 1993.

[8] S. T. Op 't Land, M. Ramdani, R. Perdriau, M. Leone, and M. Drissi, "Simple, Taylor-based worst-case model for field-to-line coupling," *JPIER*, vol. 140, pp. 297–311, 2013.

[9] U. Schulz and R. Pregla, "A new technique for the analysis of the dispersion characteristic of planar waveguides and its application to microstrip with tuning septums," *Radio Science*, vol. 16, no. 6, pp. 1173–1178, Nov. 1981.

[10] R. Pregla and W. Pascher, *Numerical Techniques for Microwave and Millimeter-Wave Passive Structures (Ch. 6)*, 1st ed. New York: Wiley, 1989.

[11] A. Zitouni, H. Bourdoucen, and T. N. Djoudi, "Quasi-static mol-based approach for the analysis of multilayer transmission line structures," *Numerical Modelling: Electronic Networks, Devices and Fields, International Journal of*, vol. 10, pp. 209–216, 1997.

[12] C. Wei, R. Barrington, J. Mautz, and T. Sarkar, "Multiconductor transmission lines in multilayered dielectric media," *Microwave Theory and Techniques, IEEE Transactions on*, vol. 32, no. 4, pp. 439–450, Apr. 1984.

[13] [Online]. Available: https://github.com/eseo-emc/field2line

[14] Z. Chen, "Examinations of higher order mode cutoff frequencies in symmetrical TEM cells," pp. 6–11, Aug. 2009.

[15] *IEEE Standard for Calibration of Electromagnetic Field Sensors and Probes, Excluding Antennas, From 9 kHz to 40 GHz*, IEEE IEEE Std 1309-2005 (Revision of IEEE Std 1309-1996), 2005.

[16] K. Malaric and J. Bartolic, "Design of a TEM-cell with increased usable test area," *Turkish Journal of Electrical Engineering and Computer Sciences*, vol. 11, no. 2, pp. 143–154, 2003.

[17] P. F. Wilson and M. T. Ma, "Simple approximate expressions for higher order mode cutoff and resonant frequencies in TEM cells," *Electromagnetic Compatibility, IEEE Transactions on*, vol. 28, no. 3, pp. 125–130, Aug. 1986.

[18] D. Hill, "Bandwidth limitation of TEM cell due to resonances," *Journal of Microwave Power*, vol. 18, pp. 181–195, Jan. 1983.